NOON States of Nine Quantized Vibrations in Two Radial Modes of a Trapped Ion

Junhua Zhang,[1,2,3,*] Mark Um,[1,†] Dingshun Lv,[1] Jing-Ning Zhang,[1] Lu-Ming Duan,[1] and Kihwan Kim[1,‡]

[1]*Center for Quantum Information, Institute for Interdisciplinary Information Sciences,*
Tsinghua University, Beijing, 100084, People's Republic of China
[2]*Shenzhen Institute for Quantum Science and Engineering, Southern University of Science and Technology,*
Shenzhen, 518055, People's Republic of China
[3]*Department of Physics, Southern University of Science and Technology, Shenzhen, 518055, People's Republic of China*

We develop a deterministic method to generate and verify arbitrarily high NOON states of quantized vibrations (phonons), through the coupling to the internal state. We experimentally create the entangled states up to $N = 9$ phonons in two vibrational modes of a single trapped $^{171}\text{Yb}^+$ ion. We observe an increasing phase sensitivity of the generated NOON state as the number of phonons N increases and obtain the fidelity from the contrast of the phase interference and the population of the phonon states through the two-mode projective measurement, which are significantly above the classical bound. We also measure the quantum Fisher information of the generated state and observe Heisenberg scaling in the lower bounds of phase sensitivity as N increases. Our scheme is generic and applicable to other photonic or phononic systems such as circuit QED systems or nanomechanical oscillators, which have Jaynes-Cummings-type of interactions.

Entangling a large number of particles has central importance for testing the boundaries and limits of quantum mechanics [1,2] and demonstrating the outperformance of quantum technologies [3]. The capability of creating a large number of entangled particles, therefore, is considered one of the benchmarks of physical platforms in developing quantum technologies. Serious theoretical and experimental developments have been dedicated to producing entanglement with a large number of particles. In various experimental platforms, including photon [4–6], trapped ion [7–9], and superconducting systems [10], a genuine multipartite entanglement of qubits, in particular, the Greenberger–Horne–Zeilinger (GHZ) state, has been prepared and verified as the benchmark.

Recently, there has been strong interest in demonstrating the power of quantum computation by using indistinguishable bosonic particles in a manner different from qubit-based universal quantum computation [11]. There has been significant experimental and technological progress [12,13], but until now, only photons have been used as the bosonic particle. However, in photonic systems, it is difficult to efficiently generate and detect single quanta, which will make it greatly challenging to exceed the computational capability of the classical computer in the near future [14]. It has been pointed out that the quantized vibration (phonon) in a trapped ion system can be an interesting resource as a bosonic particle since the generation and the measurement can be performed deterministically [15,16]. Recently, several experiments [17–20] have been demonstrated to use a phonon as a quantum resource beyond the standard role as a mediator for multiqubit operations. However, experimental developments for the full control and the measurement of phonons beyond a single vibrational mode have not yet been demonstrated much, except for a specific case [21].

Similar to the GHZ state, the quantum-mechanical many-body entangled state (NOON state) [22]

$$|\psi_{\text{NOON}}\rangle = \frac{1}{\sqrt{2}}(|N,0\rangle + e^{iN\varphi_S}|0,N\rangle) \qquad (1)$$

is a genuine multipartite entangled state with the relative phase φ_S linearly proportional to the number of indistinguishable particles N. The generation of the NOON state with a large number of particles has been experimentally pursued, mainly in photonic systems [23,24], where super-resolving phase measurements [25–28] or super-resolution quantum imaging [29,30] have been observed. In order to increase the number of photons in the NOON state and verify the state, there have been experimental endeavors such as using polarization and path degrees of freedom (d.o.f.) [25,29] or mixing quantum and classical light [27], but the schemes are generally probabilistic and the maximum number of photons in the NOON state is below $N = 6$ [27]. On the other hand, there has been an experimental attempt to use a coupling between photons and atomic internal levels to generate the NOON state [31], and a similar coupling between microwave photons and a superconducting qubit has been used to deterministically create the NOON state [32] up to $N = 3$. There have been a lot of theoretical proposals to produce a large NOON state using such nonlinear coupling [33–36]. However, these schemes

are still quite complicated and not yet experimentally demonstrated.

Here, we report a scalable and deterministic scheme to generate phononic NOON states with arbitrary number N through the coupling between vibrational d.o.f. and the internal state of an ion. We also experimentally generate the NOON state with up to $N = 9$. We introduce the new method of verifying such highly entangled states and clearly observe the super-resolution of the phase, which shows the Heisenberg scaling in the lower bound of the sensitivity provided by the quantum Fisher information. Our scheme of generation and verification of quantum states for phonon d.o.f. are generic and can be applied to any two vibrational modes through a single ion, which would be an essential tool for the large system with multiple modes [15,16,21,37].

In our experiment, we generate the NOON state in two radial modes of a $^{171}Yb^+$ ion trapped in a standard Paul trap [38], as shown in Fig. 1(a). The two radial modes are denoted as X and Y, with trap frequencies $\omega_X = (2\pi)3.2$ MHz, $\omega_Y = (2\pi)2.6$ MHz, and Lamb-Dicke parameters $\eta_X = 0.0538$, $\eta_Y = 0.0597$, which characterize the coupling strength between the internal states and the motional d.o.f. of the ion. To mediate phonon operations, two hyperfine levels of the $^{171}Yb^+$ ion in the $^2S_{1/2}$ manifold are used as a qubit, denoted as $|\downarrow\rangle \equiv |F = 0, m_F = 0\rangle$ and $|\uparrow\rangle \equiv |F = 1, m_F = 0\rangle$, which is separated by the hyperfine frequency $\omega_{HF} = (2\pi)12.6428$ GHz. The qubit can be measured by the fluorescence detection method, with $|\uparrow\rangle$ being the bright state. The state of the system is represented in Fock state basis as $|\sigma, n_X, n_Y\rangle$, where σ is the state of the qubit and n_X and n_Y are the numbers of phonons in each mode. Two laser beams from a picosecond pulsed laser with the wavelength of 355 nm shown in Fig. 1(b) are used to generate a stimulated Raman process to coherently control the internal as well as the motional states of the ion [39].

We operate the states of the ion with the combination of carrier and blue-sideband pulses described by the time evolution of the following interacting Hamiltonians, respectively [40],

$$H_C = \frac{\Omega_C}{2}(\sigma^+ + \sigma^-),$$

$$H_M = \frac{i\eta_M \Omega_M}{2}(e^{i\varphi_M}\sigma^+ a_M^\dagger - e^{-i\varphi_M}\sigma^- a_M), \quad M = X, Y, \quad (2)$$

where $\Omega_C \approx (2\pi)400$ kHz and $\eta_M \Omega_M \approx (2\pi)25$ kHz are the Rabi frequencies of carrier and blue-sideband transitions, φ_M is the phase of the driving signal, $\sigma^+ = |\uparrow\rangle\langle\downarrow|$ and $\sigma^- = |\downarrow\rangle\langle\uparrow|$, and $a_M^\dagger$ (a_M) is the creation (annihilation) operator of the motional mode M ($M = X, Y$) (see also Supplemental Material [41], Hamiltonian of the System).

Figure 2 illustrates the pulse sequence for the generation of the NOON state of $N = 3$ as an example, which is $(|\downarrow, n_X = 3, n_Y = 0\rangle + |\downarrow, 0, 3\rangle)/\sqrt{2}$ (see Supplemental Material [41], Pulse Sequence for a generalized description of the pulse sequence for arbitrary N). First, we initialize the state to $|\downarrow, 0, 0\rangle$ by the standard optical pumping technique [42] and the ground state cooling of both motional modes using the Doppler cooling and Raman-sideband cooling [43,44]. Then, we transfer the state of $|\downarrow, 0, 0\rangle$ to $|\downarrow, 1, 1\rangle$ by applying successive π pulses of blue-sideband and carrier transitions. A $\pi/2$ pulse of blue-sideband transition on the X mode is applied to change the state to $|\uparrow, 2, 1\rangle + |\downarrow, 1, 1\rangle$. Finally, two composite-pulse operations followed by a blue-sideband π pulse on the Y mode and a carrier π pulse are performed to generate the state $|\downarrow, 3, 0\rangle + |\downarrow, 0, 3\rangle$. The composite-pulse schemes are inspired by Ref. [45] and are capable of driving π transitions of the blue sideband on two different phonon
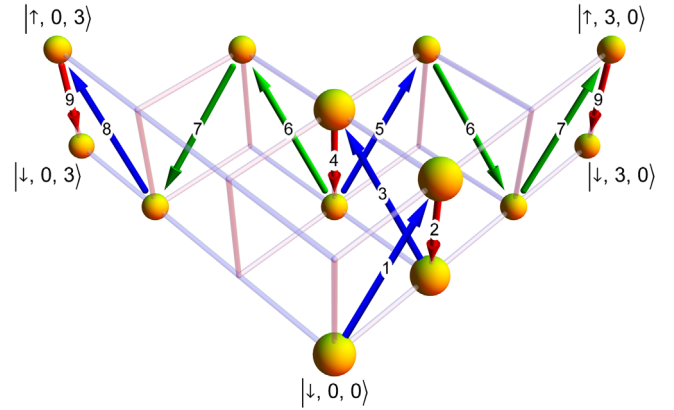
FIG. 2. Generation sequence of the NOON state of $N = 3$. The 3D grid describes the total Hilbert space of the system that consists of spin and X and Y vibrational modes. The lower and the upper layers represent $|\downarrow\rangle$ and $|\uparrow\rangle$ spin states and X and Y axes stand for the X and Y modes, where the intersection points in the grid represent the basis states as $|\sigma, n_X, n_Y\rangle$. The red arrows indicate carrier transitions, the blue arrows indicate blue-sideband transitions, and the green arrows indicate composite-pulse operations (see Supplemental Material [41], Composite Pulse). The numbers on the arrows denote the order of the operations. For example, the first blue arrow describes the blue-sideband transition on the X mode from $|\downarrow, 0, 0\rangle$ to $|\downarrow, 1, 0\rangle$.

FIG. 1. Experimental setup. (a) Side and (b) top view of the trap and laser configuration. The figures are not to scale. The diameter of the dc and rf rods and the center-to-center distance between is are 0.5 mm. The red gradient color in (a) indicates the effective two-dimensional harmonic potential in the Paul trap.

number states, which have different Rabi frequencies (see Supplemental Material [41], Composite Pulse). In order to improve the fidelity of the state, a pulse-shaping technique is applied to all blue-sideband pulses to suppress various off-resonant couplings (see Supplemental Material [41], Pulse Shaping). With the pulse sequence, we generate the NOON state up to $N = 9$, which is mainly limited by experimental imperfections that will be discussed later.

We perform the phase measurement of the NOON state between the X and Y modes by the method analogous to photonic systems, which is measuring the parity of phonon numbers in one of the output modes after the 50/50 beam splitting operations. For photons, the creation and annihilation operators of output paths after a 50/50 beam splitter are described by linear combinations of those for input paths. For phonons, we can define the similar output mode written as

$$a_O^\dagger = (a_X^\dagger + e^{i\varphi} a_Y^\dagger)/\sqrt{2},$$
$$a_O = (a_X + e^{-i\varphi} a_Y)/\sqrt{2}, \qquad (3)$$

where $\varphi = \varphi_Y - \varphi_X$ is the relative phase between X and Y modes. The parity $\Pi = \exp[i\pi a_O^\dagger a_O]$ of the output mode is constructed by measured phonon number distributions of the output mode. The phonon distribution of the output mode is measured by observing the time evolution of blue-sideband transition of the mode, which is realized by the simultaneous application of the X and Y modes blue-sideband transitions with balanced strength, $H_O = H_X + H_Y = (i\Omega_O/2)(\sigma^+ a_O^\dagger - \sigma^- a_O)$. Here, we set $\sqrt{2}\eta_X \Omega_X = \sqrt{2}\eta_Y \Omega_Y \equiv \Omega_O$. By scanning the duration of the blue-sideband transition and measuring the qubit state of the ion, the phonon distribution P_n is obtained through fitting $P_\uparrow(t) = A - \frac{1}{2}\sum_n P_n \exp[-(n+1)^{0.7}\lambda t] \times \cos[\mathcal{L}_n^1(\eta^2)\Omega t/\sqrt{n+1}]$, in which A, P_n, λ, η, and Ω are fitting parameters and $\mathcal{L}_n^1$ is an associated Laguerre polynomial [40,46]. Figure 3(b) shows a typical time evolution of the blue-sideband transition of the output mode of Eq. (3) with $\varphi = 0$, and Fig. 3(c) shows the phonon number distribution by fitting the time evolution for the NOON state of $N = 7$. The phase of the generated state ϕ_S is carefully measured and aligned with the output mode of $\varphi = 0$ (see Supplemental Material [41], Phase Alignment).

Depending on the value of φ, the oscillation of the parity is described as $\langle \Pi(\varphi) \rangle = C_P \cos N\varphi$. Figure 3(a) shows the experimental results of the parity oscillations from $N = 1$ to $N = 9$ of the generated NOON states. As shown in the fitting parameter k, the acceleration of the parity oscillation is in agreement with N within 2.6% deviation. As N increases, the contrast C_P decreases due to experimental imperfections. However, it is clearly shown that, up to $N = 9$, the contrast is over 0.5, which indicates the existence of quantum entanglement in the state.

N	k	C_P
1	1.01 ± 0.01	0.93 ± 0.02
2	2.01 ± 0.01	0.92 ± 0.02
3	2.98 ± 0.02	0.88 ± 0.02
4	4.03 ± 0.03	0.87 ± 0.02
5	4.98 ± 0.06	0.81 ± 0.03
6	6.07 ± 0.06	0.75 ± 0.03
7	7.10 ± 0.09	0.77 ± 0.03
8	7.80 ± 0.09	0.59 ± 0.02
9	9.04 ± 0.18	0.53 ± 0.04
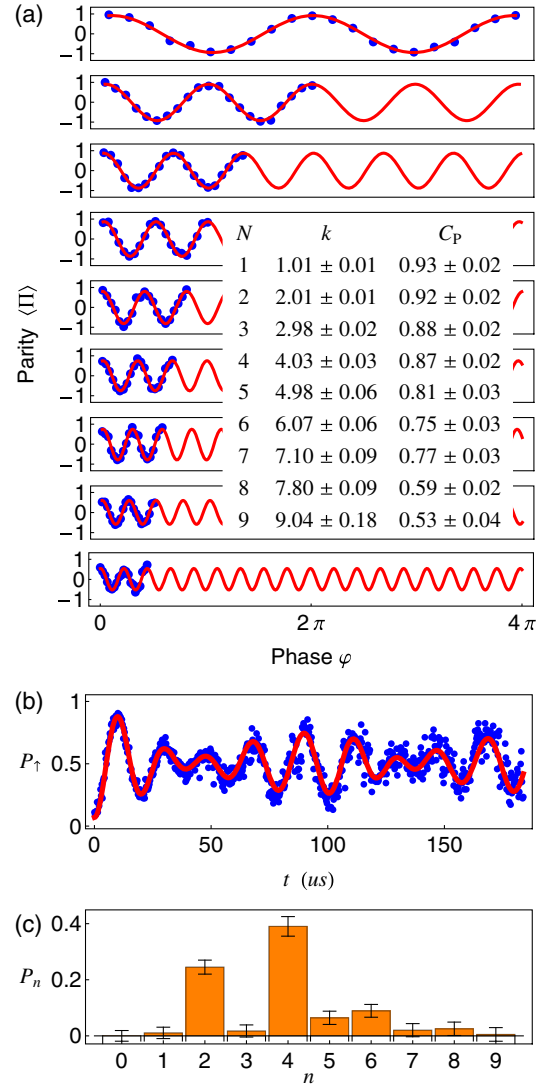
FIG. 3. Parity oscillations of the generated NOON states from $N = 1$ to $N = 9$. (a) The blue dots are experimental data, and the red lines are fitting curves with $\langle \Pi(\varphi) \rangle = A\cos k\varphi + B\sin k\varphi + C$, and $C_P = \sqrt{A^2 + B^2}$. (b) The time evolution of the blue-sideband transition of the output mode with $\varphi = 0$ for the NOON state of $N = 7$ and its fitting. (c) The corresponding phonon distribution P_n. We note that, generally, $\sum_n P_n < 1$ due to the experimental errors in the generation stage. The error bars are derived from the fitting error with a confidence level of 0.95 throughout the Letter.

We also measure the fidelity $F \equiv \langle \psi_{\text{NOON}} | \rho_{\text{exp}} | \psi_{\text{NOON}} \rangle$ of the generated NOON state. Since the density matrix of an ideal NOON state contains only two diagonal terms and two off-diagonal terms, the fidelity can be obtained by directly measuring these terms. The off-diagonal terms are proportional to the contrast of the parity oscillation $C_P = 2|\langle N, 0 | \rho_{\text{exp}} | 0, N \rangle|$ (see Supplemental Material [41], Fidelity Analysis). The diagonal terms $P_{N,0}$ and $P_{0,N}$, i.e., the populations of $|N, 0\rangle$ and $|0, N\rangle$ associated with the $|\downarrow\rangle$ state, are measured by the two-mode projective measurement that we have developed for this purpose.

The two-mode projective measurement consists of the arithmetic operations of the phonon [47] and four fluorescence detections in a single sequence of the measurement. After repeating the sequences N_{rep} times and counting $N_{X,X,X,O}$, we obtain $P_{N,0}$ (or $P_{0,N}) = N_{X,X,X,O}/N_{\text{rep}}$, the number of the cases that show no fluorescence for the first three times and fluorescence for the last detection with specifically designed arithmetic operations for the state $|N,0\rangle$ (or $|0,N\rangle$), where the internal state is projected to $|\downarrow\rangle$ ($|\uparrow\rangle$) with no fluorescence (fluorescence). The designed sequence for the state $|0,N\rangle$, for example, can be described by the following four steps from an experimentally generated state $\sum C_{p,q}|p,q\rangle|\downarrow\rangle + \sum C_{i,j}|i,j\rangle|\uparrow\rangle$. (1) No fluorescence at the first detection stage changes the state to $\sum C_{p,q}|p,q\rangle|\downarrow\rangle$. (2) With the subtraction operation on the X mode, the state is changed to $\sum_q C_{0,q}|0,q\rangle|\downarrow\rangle + \sum_{p\neq0} C_{p,q}|p-1,q\rangle|\uparrow\rangle$ and no fluorescence at the second detection stage removes all the states associated with $|\uparrow\rangle$. (3) With N times of Y mode subtraction, the state is changed to $\sum_{q\geq N} C_{0,q}|0,q-N\rangle|\downarrow\rangle + \sum_{q<N} C_{0,q}|0,N-q-1\rangle|\uparrow\rangle$ and no fluorescence at the third detection again removes $|\uparrow\rangle$ related states. (4) Finally, the one Y mode subtraction makes the state $\sum_{q>N} C_{0,q}|0,q-N-1\rangle|\downarrow\rangle + C_{0,N}|0,0\rangle|\uparrow\rangle$. Now, the fluorescence at the fourth detection is related to the state $|0,0\rangle$, which was the state $|0,N\rangle$ at the generation. Note that, in this way, if the state of the ion is projected to the target state, the recoil of the fluorescence photons only happens in the last detection stage and will not affect the result of the measurement (see Supplemental Material [41], Two-Mode Projective Measurement, for more details).

From the results of parity and population measurements, we obtain the fidelity (see Supplemental Material [41], Fidelity Analysis) of the experimental NOON state as $F = \frac{1}{2}(C_P + P_{N,0} + P_{0,N})$. As shown in Fig. 4(a), the fidelities of the NOON states up to $N = 9$ are clearly larger than 0.5, which confirms these states contain genuine multiparty entanglements.

Finally, we observe the Heisenberg scaling of the lower bound of the sensitivity in the phase estimation through the quantum Fisher information (Supplemental Material [41], Quantum Fisher Information) of the generated NOON states, shown as $F_Q = [N^2 C_P^2/(P_{N,0} + P_{0,N})]$. The quantum Fisher information provides the best possible precision on a parameter estimation given by $1/\sqrt{F_Q}$ [48,49], known as the Cramér-Rao bound. For N particles without entanglement, the best possible measurement scales as $1/\sqrt{N}$, and for the NOON state, the lower bound of the precision scales as $1/N$, the Heisenberg limit. As shown in Fig. 4(b), the lower bound of the phase uncertainty $1/\sqrt{F_Q}$ of our generated states from $N = 2$ to $N = 9$ clearly violates the classical bound and reaches the Heisenberg limit, though our states have a non-negligible amount of mixedness [50].

We also find that the maximal phase sensitivities derived from the experimental data shown in Fig. 3(a) are clearly
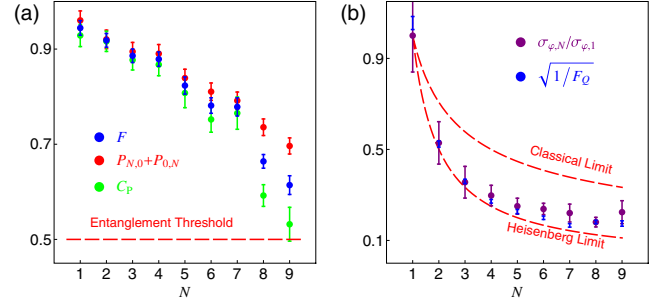
FIG. 4. Fidelity and quantum Fisher information of the generated states. (a) The experimental results of fidelity as well as C_P and $P_{N,0} + P_{0,N}$. The error bars of C_P are derived from the fitting error and those of $P_{N,0} + P_{0,N}$ from the shot-noise error. (b) The quantum Fisher information of the generated states.

below the classical limit and approach the quantum bound shown in Fig. 4(b). We obtain the phase sensitivity as $\sigma_\varphi = \sigma_\Pi/kC_p$, where σ_Π is the standard deviation of parity measurement, and k and C_p are the fitting parameters shown in Fig. 3(a). The uncertainty σ_Π of the parity measurements for each N is obtained by the average of the error bars of all the data points in Fig. 3(a), which are estimated from the fitting error bars of the phonon distributions shown in Fig. 3(b).

This scheme of generating NOON states has no principle limit on the number of phonons N. Practically, various imperfections of the system, including the fluctuation and drifting of the trap frequencies, the intensity fluctuation of Raman laser beams, and off-resonant coupling of the beams to other transitions, prohibit the increase of the number N with high fidelity. We perform numerical simulations to estimate the effect of the imperfections mentioned above. The common mode fluctuation of X and Y modes up to ±5 kHz degrade the fidelity of the NOON state with $N = 9$ by 27%, the intensity fluctuation of the laser beams in the level of 5% by 8%, and the off-resonant coupling with pulse shaping by 4%, which is qualitatively in agreement with the experimental result. We do not include the state discrimination error since we apply the correction scheme in Ref. [51]. The error from the imperfection of the ground state cooling should be less then the 1% level. We find that other errors from the coherence time of the qubit or heating of the trap are negligible in our realization.

Our generic generation and verification scheme of the NOON states can be easily applied to any quantum system that has Jaynes-Cummings interactions, including more open-geometry ion trap systems [52,53], cavity or circuit QED systems [32,54], and optomechanical systems [55]. We also emphasize that our realization of operating two vibrational modes through a single ion can be the essential component of large scale manipulations on multiple modes of multiple ions, including boson sampling of phonons. The series of the demonstrated operations through individual ions together with the phonon number resolving

detection [47,56] enables us to perform phononic boson sampling.

---

[*]zhangjh6@sustc.edu.cn
[†]ummark89@qq.com
[‡]kimkihwan@mail.tsinghua.edu.cn

[1] A. Zeilinger, Phys. Scr. **92**, 072501 (2017).
[2] A. J. Leggett, Rep. Prog. Phys. **71**, 022001 (2008).
[3] S. Boixo, S. Isakov, V. Smelyanskiy, R. Babbush, N. Ding, Z. Jiang, M. J. Bremner, J. Martinis, and H. Neven, Nat. Phys. **14**, 595 (2018).
[4] Y.-F. Huang, B.-H. Liu, L. Peng, Y.-H. Li, L. Li, C.-F. Li, and G.-C. Guo, Nat. Commun. **2**, 546 (2011).
[5] X.-C. Yao, T.-X. Wang, P. Xu, H. Lu, G.-S. Pan, X.-H. Bao, C.-Z. Peng, C.-Y. Lu, Y.-A. Chen, and J.-W. Pan, Nat. Photonics **6**, 225 (2012).
[6] X.-L. Wang, L.-K. Chen, W. Li, H.-L. Huang, C. Liu, C. Chen, Y.-H. Luo, Z.-E. Su, D. Wu, Z.-D. Li, H. Lu, Y. Hu, X. Jiang, C.-Z. Peng, L. Li, N.-L. Liu, Y.-A. Chen, C.-Y. Lu, and J.-W. Pan, Phys. Rev. Lett. **117**, 210502 (2016).
[7] C. A. Sackett, D. Kielpinski, B. E. King, C. Langer, V. Meyer, C. J. Myatt, M. Rowe, Q. A. Turchette, W. M. Itano, D. J. Wineland, and C. Monroe, Nature (London) **404**, 256 (2000).
[8] D. Leibfried, E. Knill, S. Seidelin, J. Britton, R. B. Blakestad, J. Chiaverini, D. B. Hume, W. M. Itano, J. D. Jost, C. Langer, R. Ozeri, R. Reichle, and D. J. Wineland, Nature (London) **438**, 639 (2005).
[9] T. Monz, P. Schindler, J. T. Barreiro, M. Chwalla, D. Nigg, W. A. Coish, M. Harlander, W. Hansel, M. Hennrich, and R. Blatt, Phys. Rev. Lett. **106**, 130506 (2011).
[10] C. Song, K. Xu, W. Liu, C.-P. Yang, S.-B. Zheng, H. Deng, Q. Xie, K. Huang, Q. Guo, L. Zhang, P. Zhang, D. Xu, D. Zheng, X. Zhu, H. Wang, Y.-A. Chen, C.-Y. Lu, S. Han, and J.-W. Pan, Phys. Rev. Lett. **119**, 180511 (2017).
[11] S. Aaronson and A. Arkhipov, Theory Comput. **9**, 143 (2013).
[12] J. C. Loredo, M. A. Broome, P. Hilaire, O. Gazzano, I. Sagnes, A. Lemaitre, M. P. Almeida, P. Senellart, and A. G. White, Phys. Rev. Lett. **118**, 130503 (2017).
[13] H. Wang, Y. He, Y.-H. Li, Z.-E. Su, B. Li, H.-L. Huang, X. Ding, M.-C. Chen, C. Liu, J. Qin, J.-P. Li, Y.-M. He, C. Schneider, M. Kamp, C.-Z. Peng, S. Höfling, C.-Y. Lu, and J.-W. Pan, Nat. Photonics **11**, 361 (2017).
[14] A. Neville, C. Sparrow, R. Clifford, E. Johnston, P. M. Birchall, A. Montanaro, and A. Laing, Nat. Phys. **13**, 1153 (2017).
[15] H.-K. Lau and D. F. V. James, Phys. Rev. A **85**, 062329 (2012).
[16] C. Shen, Z. Zhang, and L. M. Duan, Phys. Rev. Lett. **112**, 050504 (2014).
[17] K. Toyoda, Y. Matsuno, A. Noguchi, S. Haze, and S. Urabe, Phys. Rev. Lett. **111**, 160501 (2013).
[18] S. Ding, G. Maslennikov, R. Hablutzel, H. Loh, and D. Matsukevich, Phys. Rev. Lett. **119**, 150404 (2017).
[19] D. Kienzler, C. Flühmann, V. Negnevitsky, H.-Y. Lo, M. Marinelli, D. Nadlinger, and J. P. Home, Phys. Rev. Lett. **116**, 140402 (2016).
[20] S. Ding, G. Maslennikov, R. Hablutzel, and D. Matsukevich, Phys. Rev. Lett. **119**, 193602 (2017).
[21] K. Toyoda, R. Hiji, A. Noguchi, and S. Urabe, Nature (London) **527**, 74 (2015).
[22] B. C. Sanders, Phys. Rev. A **40**, 2417 (1989).
[23] P. Kok, H. Lee, and J. P. Dowling, Phys. Rev. A **65**, 052104 (2002).
[24] J. P. Dowling, Contemp. Phys. **49**, 125 (2008).
[25] M. W. Mitchell, J. S. Lundeen, and A. M. Steinberg, Nature (London) **429**, 161 (2004).
[26] T. Nagata, R. Okamoto, J. L. O'Brien, K. Sasaki, and S. Takeuchi, Science **316**, 726 (2007).
[27] I. Afek, O. Ambar, and Y. Silberberg, Science **328**, 879 (2010).
[28] J. C. F. Matthews, A. Politi, D. Bonneau, and J. L. O'Brien, Phys. Rev. Lett. **107**, 163602 (2011).
[29] P. Walther, J.-W. Pan, M. Aspelmeyer, R. Ursin, S. Gasparoni, and A. Zeilinger, Nature (London) **429**, 158 (2004).
[30] L. A. Rozema, J. D. Bateman, D. H. Mahler, R. Okamoto, A. Feizpour, A. Hayat, and A. M. Steinberg, Phys. Rev. Lett. **112**, 223602 (2014).
[31] Y.-A. Chen, X.-H. Bao, Z.-S. Yuan, S. Chen, B. Zhao, and J.-W. Pan, Phys. Rev. Lett. **104**, 043601 (2010).
[32] H. Wang, M. Mariantoni, R. C. Bialczak, M. Lenander, E. Lucero, M. Neeley, A. D. O'Connell, D. Sank, M. Weides, J. Wenner, T. Yamamoto, Y. Yin, J. Zhao, J. M. Martinis, and A. N. Cleland, Phys. Rev. Lett. **106**, 060401 (2011).
[33] S. T. Merkel and F. K. Wilhelm, New J. Phys. **12**, 093036 (2010).
[34] G. Nikoghosyan, M. J. Hartmann, and M. B. Plenio, Phys. Rev. Lett. **108**, 123603 (2012).
[35] S. S. Ivanov, N. V. Vitanov, and N. V. Korolkova, New J. Phys. **15**, 023039 (2013).
[36] Q.-P. Su, C.-P. Yang, and S.-B. Zheng, Sci. Rep. **4**, 3898 (2014).
[37] L. Ortiz-Gutiérrez, B. Gabrielly, L. F. Muñoz, K. T. Pereira, J. G. Filgueiras, and A. S. Villar, Opt. Commun. **397**, 166 (2017).
[38] W. Paul, Rev. Mod. Phys. **62**, 531 (1990).
[39] D. Hayes, D. N. Matsukevich, P. Maunz, D. Hucul, Q. Quraishi, S. Olmschenk, W. Campbell, J. Mizrahi, C. Senko, and C. Monroe, Phys. Rev. Lett. **104**, 140501 (2010).
[40] D. Leibfried, R. Blatt, C. Monroe, and D. Wineland, Rev. Mod. Phys. **75**, 281 (2003).
[41] See Supplemental Material at http://link.aps.org/supplemental/10.1103/PhysRevLett.121.160502 for further details on experimental implementations and methods of data analysis. It contains the description of detailed pulse

sequence for the creation of NOON state including composite pulses, phase adjustment, and two-mode projective measurements and the discussion of the fidelity measurement and fisher information.

[42] S. Olmschenk, K. C. Younge, D. L. Moehring, D. N. Matsukevich, P. Maunz, and C. Monroe, Phys. Rev. A **76**, 052314 (2007).

[43] C. Monroe, D. M. Meekhof, B. E. King, W. M. Itano, and D. J. Wineland, Phys. Rev. Lett. **75**, 4714 (1995).

[44] C. Roos, T. Zeiger, H. Rohde, H. C. Nägerl, J. Eschner, D. Leibfried, F. Schmidt-Kaler, and R. Blatt, Phys. Rev. Lett. **83**, 4713 (1999).

[45] F. Schmidt-Kaler, H. Haffner, M. Riebe, S. Gulde, G. P. T. Lancaster, T. Deuschle, C. Becher, C. F. Roos, J. Eschner, and R. Blatt, Nature (London) **422**, 408 (2003).

[46] D. M. Meekhof, C. Monroe, B. E. King, W. M. Itano, and D. J. Wineland, Phys. Rev. Lett. **76**, 1796 (1996).

[47] M. Um, J. Zhang, D. Lv, Y. Lu, S. An, J.-N. Zhang, H. Nha, M. S. Kim, and K. Kim, Nat. Commun. **7**, 11410 (2016).

[48] S. L. Braunstein and C. M. Caves, Phys. Rev. Lett. **72**, 3439 (1994).

[49] J. J. Cooper and J. A. Dunningham, New J. Phys. **13**, 115003 (2011).

[50] K. Modi, H. Cable, M. Williamson, and V. Vedral, Phys. Rev. X **1**, 021022 (2011).

[51] C. Shen and L. M. Duan, New J. Phys. **14**, 053053 (2012).

[52] S. Seidelin, J. Chiaverini, R. Reichle, J. J. Bollinger, D. Leibfried, J. Britton, J. H. Wesenberg, R. B. Blakestad, R. J. Epstein, D. B. Hume, W. M. Itano, J. D. Jost, C. Langer, R. Ozeri, N. Shiga, and D. J. Wineland, Phys. Rev. Lett. **96**, 253003 (2006).

[53] R. Maiwald, D. Leibfried, J. Britton, J. C. Bergquist, G. Leuchs, and D. J. Wineland, Nat. Phys. **5**, 551 (2009).

[54] Q.-P. Su, C.-P. Yang, and S.-B. Zheng, Sci. Rep. **4**, 3898 (2014).

[55] M. Aspelmeyer, T. J. Kippenberg, and F. Marquardt, Rev. Mod. Phys. **86**, 1391 (2014).

[56] S. An, J. N. Zhang, M. Um, D. Lv, Y. Lu, J. Zhang, Z.-Q. Yin, H. T. Quan, and K. Kim, Nat. Phys. **11**, 193 (2015).